Entangled end states with fractionalized spin projection in a time-reversal-invariant topological superconducting wire

Armando A. Aligia[1] and Liliana Arrachea[2]

[1]*Centro Atómico Bariloche and Instituto Balseiro, CNEA, 8400 S. C. de Bariloche, Argentina*

[2]*International Center for Advanced Studies, ECyT-UNSAM, Campus Miguelete, 25 de Mayo y Francia, 1650 Buenos Aires, Argentina*

(Received 24 June 2018; revised manuscript received 24 August 2018; published 20 November 2018)

We study the ground state and low-energy subgap excitations of a finite wire of a time-reversal-invariant topological superconductor (TRITOPS) with spin-orbit coupling. We solve the problem analytically for a long chain of a specific one-dimensional lattice model in the electron-hole symmetric configuration and numerically for other cases of the same model. We present results for the spin density of excitations in long chains with an odd number of particles. The total spin projection along the axis of the spin-orbit coupling $S_z = \pm 1/2$ is distributed with fractions $\pm 1/4$ localized at both ends and shows even-odd alternation along the sites of the chain. We calculate the localization length of these excitations and find that it can be well approximated by a simple analytical expression. We show that the energy E of the lowest subgap excitations of the finite chain defines tunneling and entanglement between end states. We discuss the effect of a Zeeman coupling Δ_Z on one of the ends of the chain only. For $\Delta_Z < E$, the energy difference of excitations with opposite spin orientation is $\Delta_Z/2$, consistent with a spin projection $\pm 1/4$. We argue that these physical features are not model dependent and can be experimentally observed in TRITOPS wires under appropriate conditions.

DOI: 10.1103/PhysRevB.98.174507

I. INTRODUCTION

Topological materials including topological superconductors (TS) are a subject of great interest recently in condensed matter physics. This field of research had a burst after the observation by Kitaev that a one-dimensional model of spinless fermions with p-wave BCS pairing has a topological phase with zero-energy subgap excitations that are described by Majorana fermions [1]. The non-abelian statistics obeyed by these quasiparticles is an appealing property for implementing quantum computing protocols. Since then, several proposals for realizing this phase in concrete physical systems were formulated. In particular, quantum superconducting wires with spin-orbit coupling and magnetic field [2–8], edge states of the quantum spin Hall state in proximity to superconductors and in contact to magnetic moments [9] and Shiba states induced by magnetic adatoms on superconducting substrates [10]. All these mechanisms to generate the topological superconducting phase contain ingredients breaking time-reversal symmetry.

In contrast, there is another family of TS, the time-reversal-invariant topological superconductors (TRITOPS) where the zero-mode edge excitations appear in Kramers pairs [11–20]. This property has interesting implications which can be relevant for their detection and manipulation [21–26]. For a recent review on proposals to realize the TRITOPS phase, see Ref. [27]. In particular, Zhang *et al.* [12] proposed to engineer one- and two-dimensional TRITOPS via proximity effect between nodeless extended s-wave iron-based superconductors and semiconducting systems with large Rashba spin-orbit interactions. A sketch of a one-dimensional (1D) setup is shown in Fig. 1. At each end of a long TRITOPS wire, there is a Kramers pair of Majorana edge states at zero energy. For a finite wire, there is a mixing of the end states and the four fermions of zero energy split in two pairs with energy $\pm E$. One of the interesting properties of this family is the fact that subgap excitations were argued to have fractional spin projection along the direction of the spin-orbit coupling z [13]. This has consequences in the physical behavior of these systems when put in contact to magnetic systems. An example is the quench of the $0 - \pi$ transition in the Josephson current of a quantum dot embedded in a TRITOPS junction [23].

In this work we study these low-energy end states of a finite chain. By using a method presented recently by Alase *et al.* [28,29] we analytically calculate the zero-energy eigenstates of an infinite chain of the model introduced by Zhang *et al.* in Ref. [12] in the particle-hole symmetric configuration of the normal system (which means that the chemical potential $\mu = 0$). This corresponds to the explicit solution of the Kramers pairs of Majorana edge states. We calculate the localization length of the low-energy excitations for arbitrary μ. We also find analytical explicit expressions for these states in the case of finite chains with $\mu = 0$ and complement our study with some numerical results for other values of μ. In finite chains with an odd number of particles, there is an effective tunneling which entangles the end states. This stabilizes a ground state in which the spin projection at each end is $S_e^z = \pm 1/4$ [$e = L$ (left) or $e = R$ (right)]. Instead, for systems with an even number of particles, $S_e^z = 0$. We show that the parameter characterizing the tunneling is, precisely, the energy E of the lowest subgap excitations. We also calculate the distribution of S_z along the chain. In addition, we analyze the response to Zeeman coupling Δ_Z induced by a weak magnetic field or an Ising coupling with a magnetic moment, acting on one of the edges of the wire, as sketched in Fig. 1. We show that in short enough chains where the excitations at both ends are entangled, the fractionalization of S_z manifests itself in a Zeeman splitting of half the amplitude of the usual one for spin 1/2. The condition to observe this fractional Zeeman

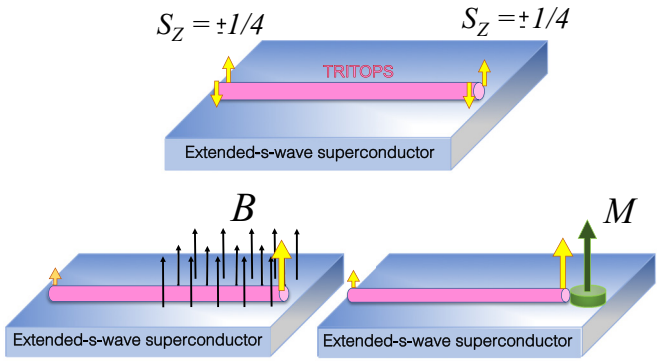

FIG. 1. Sketch of the setup. Top: Excited subgap states with total spin projection $S_z = 1/2$ of a TRITOPS wire with spin-orbit coupling, where superconductivity is induced by proximity to a macroscopic superconductor with extended s-wave pairing. Spin projection is fractionalized with $S_e^z = 1/4$ localized at the ends of the wire. Bottom: a weak magnetic field B in the direction of the spin-orbit coupling is applied at the right side of the setup, inducing polarization of the subgap mode (left). Alternatively, one of the subgap modes interacts with a magnetic island with magnetic moment M (right).

response is $\Delta_Z < E$. For long chains with $\Delta_Z \gg E$, the spin projection at each end remains $S_e^z = \pm 1/4$ depending on the total spin projection $S_z = \pm 1/2$ for odd number of particles, while it evolves to $S_L^z = -S_R^z = \pm 1/4$ for even number of particles. Importantly, although we solve a specific model, the physical behavior related to the distribution of S_z and response is generic of any TRITOPS wire.

The finite energy of these odd parity states might be detected in experiments where capacitance effects permit to control the charge in small superconducting islands [30]. In these systems also the chemical potential μ can be controlled by a gate voltage. The Zeeman spitting can also be detected by scanning tunneling spectroscopy experiments akin to those performed to observe Shiba states induced by magnetic adatoms in superconducting substrates [31–33]. Finally also microwave excitations [34,35] in a finite chain with odd number of particles might detect the anomalous (half) Zeeman splitting of the low-energy excitations.

The paper is organized as follows. In Sec. II the model is described. In Sec. III we present the approach to analytically diagonalize it for $\mu = 0$. In Sec. IV we show the dependence on the localization length with μ and compare with a simple analytical approximation. Section V contains analytical and numerical results for the spin projection S_i^z at each site i for a finite wire with odd number of particles. In Sec. VII we calculate the effect of a magnetic field at one end of the chain. In Sec. VIII we present a summary and a brief discussion.

II. MODEL

The TRITOPS chain is described by the Hamiltonian proposed in Ref. [12],

$$H = \sum_{j=1}^{L} \sum_{\sigma} [-t c_{j+1\sigma}^{\dagger} c_{j\sigma} - \mu\, c_{j\sigma}^{\dagger} c_{j\sigma} + i\lambda_{\sigma} c_{j+1\sigma}^{\dagger} c_{j\sigma} + (\Delta_{\sigma} e^{i\phi} c_{j+1\sigma}^{\dagger} c_{j\overline{\sigma}}^{\dagger} + \text{H.c.})], \quad (1)$$

where $\lambda_{\uparrow,\downarrow} = \pm\lambda$, $\Delta_{\uparrow,\downarrow} = \pm\Delta$, and $\overline{\uparrow} = \downarrow$, $\overline{\downarrow} = \uparrow$. The first term corresponds to nearest-neighbor hopping, μ is the chemical potential, and λ and Δ are the strengths of Rashba spin-orbit coupling and extended s-wave pairing, respectively.

For completeness, we include in the Hamiltonian the phase ϕ, which is important when the chain is coupled in a Josephson circuit, although it does not play an important role in the behavior of the spin excitations [12,23,24,36]. For $\phi = 0$, the Hamiltonian is invariant under time-reversal symmetry. In addition, in absence of superconductivity ($\Delta = 0$), for $\mu = 0$, the Hamiltonian is invariant under the electron hole transformation $c_{j\sigma}^{\dagger} \to (-1)^j c_{j\sigma}$.

While H supports topological and nontopological phases, in our work we are interested in the topological phase that takes place for $|\mu| < 2|\lambda|$. In Ref. [12] a local s-wave pairing Δ_0 was also considered. Since the topological phase exists for dominant nearest-neighbor pairing ($|\Delta_0| < |\Delta|$), for simplicity we focus on the case $\Delta_0 = 0$. In this phase when the number of sites $L \to \infty$, there is a Kramers pair of Majorana fermions at each end with energy $E = 0$. For a finite chain the end states mix as described in the following sections.

III. DIAGONALIZATION OF THE CHAIN WITH ARBITRARY BOUNDARY CONDITIONS

In this section, we discuss the application of the method presented in Refs. [28,29] by Alase *et al.* to diagonalize a 1D noninteracting homogeneous Hamiltonian with arbitrary boundary conditions. Then, we study the particular case of an electron-hole symmetric band ($\mu = 0$) for which an analytical result for the zero-energy eigenstates for $L \to \infty$ is derived. Finally, we also obtain analytically the low-energy eigenstates for $\mu = 0$ and a long finite chain. Those readers who are not interested in the derivation can skip this section and go directly to the analytical results for $\mu = 0$: Eq. (18) and the following for the zero-energy modes of the infinite chain and Eq. (38) and the following for the low-energy modes of the finite chain.

A. Formalism for the general case

Here we we discuss the application of the method of Alase *et al.* to the model of Eq. (1). For those readers who are more familiar with Nambu notation, an alternative version of the procedure is presented in the Appendix.

To simplify the use of the method of Alase *et al.* [28,29], it is convenient to map the model with M spin-orbitals α ($M = 2L$ in our case) to one expressed in terms of $2M$ kets associated with the annihilation (a) and creation (c) operators:

$$c_{\alpha} \leftrightarrow |\alpha a\rangle, c_{\alpha}^{\dagger} \leftrightarrow |\alpha c\rangle. \quad (2)$$

The ensuing Hamiltonian is

$$\tilde{H} = \sum_{\beta\alpha} (A_{\beta\alpha} |\beta a\rangle\langle\alpha a| + B_{\beta\alpha} |\beta c\rangle\langle\alpha a| - \overline{A}_{\beta\alpha} |\beta c\rangle\langle\alpha c| + \overline{B}_{\beta\alpha} |\beta a\rangle\langle\alpha c|), \quad (3)$$

with $\overline{A}_{\beta\alpha} = A^*_{\beta\alpha}$ and $\overline{B}_{\beta\alpha} = B^*_{\beta\alpha}$. These matrix elements are defined from the equations

$$[c_\alpha, H] = \sum_\beta (A_{\beta\alpha} c_\beta + B_{\beta\alpha} c^\dagger_\beta). \tag{4}$$

Hence,

$$\begin{aligned} \tilde{H}|\alpha a\rangle &= \sum_\beta (A_{\beta\alpha}|\beta a\rangle + B_{\beta\alpha}|\beta c\rangle), \\ \tilde{H}|\alpha c\rangle &= -\sum_\beta (\bar{A}_{\beta\alpha}|\beta c\rangle + \bar{B}_{\beta\alpha}|\beta d\rangle). \end{aligned} \tag{5}$$

Thus, we see that solving Eq. (5) is equivalent to solving Eq. (4).

In this notation we define projection operators over bulk (P_B) and boundary ($P_{\rm bou}$) states with $P_B + P_{\rm bou} = 1$. The projector P_B is over all those sites in which all the hopping terms are contained in the chain. In our case,

$$\begin{aligned} P_B &= \sum_{j=2}^{L-1} P_j, \\ P_{\rm bou} &= P_1 + P_L, \\ P_j &= \sum_\sigma (|j\sigma a\rangle\langle j\sigma a| + |j\sigma c\rangle\langle j\sigma c|). \end{aligned} \tag{6}$$

Following again Alase et al. [28,29], we construct generalized Bloch functions which permit us to solve the bulk eigenvalue problem $P_B \tilde{H}|e\rangle = E P_B|e\rangle$ for certain roots $z(E)$. Finally, the equation $P_{\rm bou}\tilde{H}|e\rangle = P_{\rm bou} E|e\rangle$ determines the allowed energies E and the eigenstates $|e\rangle$. Specifically, for our problem the four generalized Bloch states can be written as

$$|z\sigma o\rangle = w_z \sum_{j=1}^{L} z^{j-1}|j\sigma o\rangle, \tag{7}$$

where $o = a$ or c, $\sigma = \uparrow$ or $\downarrow$, w_z is the coefficient of $|j\sigma o\rangle$, and z is a complex number to be determined later.

Using Eqs. (1), (4), (5), (6), and (7) and some algebra we get

$$\begin{aligned} P_B\tilde{H}|z\uparrow a\rangle &= \left[-\mu - t\left(z+\frac{1}{z}\right) + i\lambda\left(z-\frac{1}{z}\right)\right] P_B|z\uparrow a\rangle \\ &\quad + \Delta e^{i\phi}\left(z+\frac{1}{z}\right) P_B|z\downarrow c\rangle, \\ P_B\tilde{H}|z\downarrow c\rangle &= \left[\mu + t\left(z+\frac{1}{z}\right) - i\lambda\left(z-\frac{1}{z}\right)\right] P_B|z\downarrow c\rangle \\ &\quad + \Delta e^{-i\phi}\left(z+\frac{1}{z}\right) P_B|z\uparrow a\rangle. \end{aligned} \tag{8}$$

Similar equations are obtained interchanging $\uparrow$ and $\downarrow$ and simultaneously changing the sign of both, λ and Δ.

Using Eqs. (8), and the ansatz $|e\rangle = u|z\uparrow a\rangle + v|z\downarrow c\rangle$, the bulk eigenvalue problem $P_B(\tilde{H} - E)|e\rangle = 0$ takes the form

$$\begin{pmatrix} a(z) - E & b(z)e^{-i\phi} \\ b(z)e^{i\phi} & -a(z) - E \end{pmatrix}\begin{pmatrix} u(z) \\ v(z) \end{pmatrix} = 0, \tag{9}$$

where

$$\begin{aligned} a(z) &= -\mu - t\left(z+\frac{1}{z}\right) + i\lambda\left(z-\frac{1}{z}\right), \\ b(z) &= \Delta\left(z+\frac{1}{z}\right). \end{aligned} \tag{10}$$

Vanishing of the determinant of the matrix implies

$$\begin{aligned} E^2 &= \mu^2 + (t^2+\Delta^2)\left(z+\frac{1}{z}\right)^2 - \lambda^2\left(z-\frac{1}{z}\right)^2 \\ &\quad + 2\mu t\left(z+\frac{1}{z}\right) \\ &\quad - 2i\lambda\left[\mu\left(z-\frac{1}{z}\right) + t\left(z^2-\frac{1}{z^2}\right)\right]. \end{aligned} \tag{11}$$

For each energy E, there are four solutions $z_k(E)$ of this equation, which lead to four eigenstates $|e_k\rangle$ of the bulk equation with $u_k > 0$ and

$$\frac{v_k}{u_k} = \frac{e^{i\phi}(E - a_k)}{b_k}. \tag{12}$$

Here we have introduced the notation $a_k \equiv a(z_k)$, $b_k \equiv b(z_k)$, $u_k \equiv u_\sigma(z_k)$, and $v_k \equiv v_\sigma(z_k)$.

The solution of the full eigenvalue equation $(\tilde{H} - E)|f\rangle = 0$ has the form $|f\rangle = \sum \alpha_k |e_k\rangle$. The coefficients α_k and the energy E are determined by the boundary equations $P_{\rm bou}(\tilde{H} - E)|f\rangle = 0$. For our problem, $P_1(\tilde{H} - E)|f\rangle = 0$ and $P_L(\tilde{H} - E)|f\rangle = 0$ implies

$$\begin{aligned} \sum_{k=1}^{4}\left[(a_k^1 - E)u_k + b_k^1 e^{-i\phi} v_k\right]\alpha_k &= 0, \\ \sum_{k=1}^{4}\left[u_k b_k^1 e^{i\phi} - (a_k^1 + E)v_k\right]\alpha_k &= 0, \\ \sum_{k=1}^{4}\left[(a_k^L - E)u_k + b_k^L e^{-i\phi} v_k\right]\alpha_k &= 0, \\ \sum_{k=1}^{4}\left[b_k^L e^{i\phi} u_k - (a_k^L + E)v_k\right]\alpha_k &= 0, \end{aligned} \tag{13}$$

with the definitions

$$\begin{aligned} a_k^1 &= w_k(-\mu - t z_k + i\lambda z_k), \\ a_k^L &= w_k\left(-\mu - \frac{t}{z_k} - i\frac{\lambda}{z_k}\right) z_k^{L-1}, \\ b_k^1 &= w_k \Delta z_k, \qquad b_k^L = w_k \Delta z_k^{L-2}. \end{aligned} \tag{14}$$

Interchanging $\uparrow$ and $\downarrow$ and simultaneously changing the sign of both, λ and Δ, or directly applying the time-reversal operator for $\phi = 0$, eigenstates (degenerate with the previous ones) which involve linear combinations of the form $u|z\downarrow a\rangle + v|z\uparrow c\rangle$ are obtained.

B. Solution for $\mu = 0$, $L \to \infty$, $E \to 0$

In general, for finite wires, the chemical potential μ can be adjusted using a gate voltage. For $\mu = 0$, Eq. (11) can be

solved analytically. In fact, for $\mu = 0$ the odd powers of z in Eq. (11) disappear and the ensuing equation is quadratic in z^2. This value of the chemical potential is within the topological phase, which is characterized by Kramers pairs of Majorana zero modes localized at the ends of the chain. These states are exactly at $E = 0$ only in the limit of an infinitely long chain, where they are completely decoupled. We discuss this limit here since this solution sheds light on the structure and properties of these states. In particular for $t \to 0$, $|\Delta| = |\lambda|$ a very simple solution is found, which involves operators at sites 1 and L only. We postpone the discussion of the effect of the finite length of the chain for the next subsection.

Note that for any μ, Eq. (11) is invariant under the simultaneous change of sign of λ and $z \leftrightarrow 1/z$. In addition, if z is a solution of Eq. (11), its complex conjugate $\bar{z}$ is a solution of the same equation for the opposite sign of λ. Combining both properties one realizes that if z is a solution of Eq. (11), then $1/\bar{z}$ is also a solution. For $\mu = 0$, if z is a solution, then $-z$ is also a solution. This implies that knowing one solution of Eq. (11), which we call z_1, the others are related to it as follows:

$$z_2 = -z_1, \; z_3 = \frac{1}{\bar{z}_1}, \; z_4 = -z_3. \tag{15}$$

For $E = 0$ two solutions have $|z| < 1$ and the other two $|z| > 1$. Choosing z_1 as one of the solutions satisfying $|z_1| < 1$, we obtain after some algebra

$$z_1^2 = z_2^2 = -\frac{t^2 + (|\Delta| - |\lambda|)^2}{\Delta^2 + (t - i\lambda)^2}. \tag{16}$$

Then, the amplitude of $|j\sigma o\rangle$ in the states $|e_k\rangle$ with $k = 1, 2$ ($k = 3, 4$) decrease (increase) exponentially as j increases. In the limit where $L \to \infty$ we can separate the states localized at each end. For the left one (low j) only $k = 1, 2$ matter. Using Eq. (12) we obtain

$$\frac{v_1}{u_1} = \frac{v_2}{u_2} = p, \tag{17}$$

where we define

$$p = ie^{i\phi}\text{sign}(\Delta\lambda). \tag{18}$$

We also define $w_k = 1/u_k$ and normalize the states at the end of the calculation. With this choice, the last two Eqs. (13) lead to $a_2^1 = -a_1^1$, $b_2^1 = -b_1^1$, and the first two Eqs. (13) lead to $\alpha_2 = \alpha_1$. In terms of the original fermionic operators, the normalized solution for the zero-energy $\uparrow$ spin excitation localized at the left end reads

$$\gamma_\uparrow = N \sum_{n=0}^{\infty} z_1^{2n}(c_{2n+1\uparrow} + p c_{2n+1\downarrow}^\dagger),$$
$$N = \left(\frac{1 - |z_1|^4}{2}\right)^{1/2}. \tag{19}$$

Similarly, interchanging $\uparrow$ and $\downarrow$ and inverting the signs of λ and Δ we have

$$\gamma_\downarrow = N \sum_{n=0}^{\infty} \bar{z}_1^{2n}(c_{2n+1\downarrow} + p c_{2n+1\uparrow}^\dagger), \tag{20}$$

which corresponds to the Kramers partner of Eq. (19). Surprisingly, the even sites do not enter these Eqs. In addition, note that

$$\gamma_\uparrow^\dagger = \bar{p}\gamma_\downarrow, \qquad \gamma_\downarrow^\dagger = \bar{p}\gamma_\uparrow. \tag{21}$$

Then, it is possible to define two independent Majorana operators,

$$\eta_1 = \gamma_\uparrow^\dagger + \gamma_\uparrow, \qquad \eta_2 = i(\gamma_\uparrow^\dagger - \gamma_\uparrow), \tag{22}$$

such that $\eta_i^\dagger = \eta_i$.

A particular simple case is $t \to 0$, $|\Delta| = |\lambda|$, for which $z \to 0$ [see Eq. (16)] and then Eqs. (19) and (20) reduce to

$$\gamma_\sigma = \frac{1}{\sqrt{2}}(c_{1\sigma} + p c_{1-\sigma}^\dagger). \tag{23}$$

It can be verified directly that for these parameters, $[\gamma_\sigma, H] = 0$.

We can proceed in a similar way to derive the zero-energy excitations localized at the right end. Using Eqs. (10), (12), and (15) we obtain

$$\frac{v_3}{u_3} = \frac{v_4}{u_4} = -p. \tag{24}$$

Then, using Eqs. (14), the right-end eigenstates of zero energy can be expressed in terms of fermionic operators as

$$\tilde{\gamma}_\uparrow = N \sum_{n=0}^{\infty} \bar{z}_1^{2n}(c_{L-2n\uparrow} - p c_{L-2n\downarrow}^\dagger),$$
$$\tilde{\gamma}_\downarrow = N \sum_{n=0}^{\infty} z_1^{2n}(c_{L-2n\downarrow} - p c_{L-2n\uparrow}^\dagger). \tag{25}$$

Similar to the left-end excitations, they are related by

$$\tilde{\gamma}_\uparrow^\dagger = -\bar{p}\tilde{\gamma}_\downarrow, \tilde{\gamma}_\downarrow^\dagger = -\bar{p}\tilde{\gamma}_\uparrow. \tag{26}$$

C. Properties of the end excitations of the infinite chain

The relations given by Eqs. (21) and (26) imply

$$\{\gamma_\uparrow, \gamma_\downarrow\} = p, \; \{\tilde{\gamma}_\uparrow, \tilde{\gamma}_\downarrow\} = -p. \tag{27}$$

Denoting by $\hat{\gamma}_\sigma$ any of the two operators γ_σ, $\tilde{\gamma}_\sigma$, it is easy to verify that

$$[\hat{\gamma}_\sigma, S_z] = (s/2)\hat{\gamma}_\sigma, \tag{28}$$

where $s = 1$ (-1) for $\sigma = \uparrow$ $(\downarrow)$ and $S_z = \sum_i (c_{i\uparrow}^\dagger c_{i\uparrow} - c_{i\downarrow}^\dagger c_{i\downarrow})/2$ is the total spin projection in the Rashba direction z. Using Eq. (28) it is easy to see that rotating the operator $\hat{\gamma}_\sigma$ an angle φ around z one obtains

$$\exp(-i\varphi S_z)\hat{\gamma}_\sigma \exp(i\varphi S_z) = \exp(si\varphi/2)\hat{\gamma}_\sigma. \tag{29}$$

Then $\hat{\gamma}_\uparrow$ $(\hat{\gamma}_\downarrow)$ transforms like a spin with $S_z = -1/2$ $(1/2)$ under rotations around z. Note, however, that due to the Rashba spin-orbit coupling, the total spin is not conserved. For example, one has

$$[\gamma_\uparrow, S_x] = \frac{N}{2} \sum_{n=0}^{\infty} z_1^{2n}(c_{2n+1\downarrow} - p c_{2n+1\uparrow}^\dagger), \tag{30}$$

and the second member anticommutes with all low-energy operators $\hat{\gamma}_\sigma$. This is also true for S_y and the rest of the $\hat{\gamma}_\sigma$ operators.

The end excitations described by $\gamma_\sigma, \tilde{\gamma}_\sigma$ satisfy the usual Pauli exclusion principle $\gamma_\sigma^2 = \tilde{\gamma}_\sigma^2 = 0$. Hence, taking into account the relations of Eqs. (21) and (26), we can characterize the end states by two operators, $\gamma \equiv \gamma_\uparrow$ and $\tilde{\gamma} \equiv \tilde{\gamma}_\uparrow$. These operators define q-bit states $|L0\rangle$, $|L1\rangle$, localized at the left edge and $|R0\rangle$, $|R1\rangle$, localized at the right, satisfying

$$\begin{aligned} \gamma|L0\rangle &= 0, \qquad |L1\rangle = \gamma^\dagger|L0\rangle, \\ \tilde{\gamma}|R0\rangle &= 0, \qquad |R1\rangle = \tilde{\gamma}^\dagger|R0\rangle. \end{aligned} \tag{31}$$

Equations (16), (19), (20), and (25) define the zero-energy excitations of the infinite chain. For finite odd L, the corresponding operators continue to commute with the Hamiltonian [37]. This means that the zero-energy excitations persist. This is a particular property of the case $\mu = 0$. For even finite L, the states γ_σ and $\tilde{\gamma}_\sigma$ mix as described in the next section.

D. Extension to finite large even L

For finite odd L, as long as $\mu = 0$, the edge states have the same properties as those of $L \to \infty$. Namely, they have exactly energy $E = 0$, and they can be expressed as in Eqs. (19), (20), and (25). For finite even L, the left and right zero modes discussed in the previous section hybridize and the resulting subgap eigenstates have finite energy $\pm E$, which decreases exponentially with L. For even L, the first correction to the solution presented in the previous section is of order $E \sim |z_1|^L$. From Eq. (11) we see that the first correction to the roots z_i is of order E^2. Then, to linear order in E, the z_i are not modified. However, Eqs. (10) and (12) are linear in E. Explicitly, after substituting the solution of Eq. (16) and the definition of Eq. (18) they read

$$\begin{aligned} \frac{v_1}{u_1} &= p + \frac{e^{i\phi}E}{\Delta\left(z_1 + \frac{1}{z_1}\right)}, \\ \frac{v_2}{u_2} &= p - \frac{e^{i\phi}E}{\Delta\left(z_1 + \frac{1}{z_1}\right)}, \\ \frac{v_3}{u_3} &= -p + \frac{e^{i\phi}E}{\Delta\left(\bar{z}_1 + \frac{1}{\bar{z}_1}\right)}, \\ \frac{v_4}{u_4} &= -p - \frac{e^{i\phi}E}{\Delta\left(\bar{z}_1 + \frac{1}{\bar{z}_1}\right)}. \end{aligned} \tag{32}$$

As we know from the previous Section, for $L \to \infty$, $E = 0$, the two ends are decoupled and Eqs. (13) and (14) give $\alpha_2 = \alpha_1, \alpha_4 = \alpha_3$ for the coefficients of the eigenstate $\sum \alpha_k |e_k\rangle$. We define two deviations from this limit, linear in E, $\beta_1 = \alpha_2 - \alpha_1$, $\beta_3 = \alpha_4 - \alpha_3$. Choosing $w_k = 1/u_k$ for $k = 1, 2$ (weight 1 for $c_{1\uparrow}$) and $w_k = z_k^{1-L}/u_k$ for $k = 3, 4$ (weight 1 for $c_{L\uparrow}$), the linear corrections in E to Eqs. (13) lead to the following equations [37]:

$$\begin{aligned} 0 = {} & 2\alpha_1 E\left[\frac{z_1}{\left(z_1 + \frac{1}{z_1}\right)} - 1\right] \\ & + 2\alpha_3 \bar{z}_1^{L-2}[-t + i\lambda - pe^{-i\phi}\Delta] \\ & + \beta_1 z_1[t - i\lambda - pe^{-i\phi}\Delta], \end{aligned} \tag{33}$$

$$\begin{aligned} 0 = {} & -2\alpha_1 E\left[p + \frac{(-t + i\lambda)e^{i\phi}z_1}{\Delta\left(z_1 + \frac{1}{z_1}\right)}\right] \\ & + 2\alpha_3 \bar{z}_1^{L-2}[(-t + i\lambda)p + e^{i\phi}\Delta] \\ & - \beta_1 z_1[p(t - i\lambda) + e^{i\phi}\Delta]. \end{aligned} \tag{34}$$

From these expressions, β_1 can be eliminated leaving an equation that relates α_1 and α_3. In fact, β_1 turns out to be exponentially small and we neglect it. More precisely, performing the operation Eq. (34) + Eq. (33)$/p$ and substituting Eq. (18), results in the following relation between α_1 and α_3:

$$Ey\alpha_1 + x\alpha_3 = 0, \tag{35}$$

where

$$\begin{aligned} y &= 1 + \frac{i\,\mathrm{sign}(\Delta\lambda)(t - i\lambda)z_1^2 + \Delta}{\left(z_1^2 + 1\right)\Delta}, \\ x &= \bar{z}_1^{L-2}\varepsilon, \qquad \varepsilon = 2[t - i\lambda + i\,\mathrm{sign}(\Delta\lambda)\Delta]. \end{aligned} \tag{36}$$

We can follow a similar procedure to evaluate the linear corrections in E to Eqs. (14). The result is

$$\bar{x}\alpha_1 + E\bar{y}\alpha_3 = 0. \tag{37}$$

From Eqs. (35) and (37) we finally obtain the desired energy and the ratio α_3/α_1, which has modulo 1. For the energy, we get

$$E = \pm\left|\frac{x}{y}\right| = \pm\left|\frac{\bar{z}_1^{L-2}\varepsilon}{y}\right|, \tag{38}$$

which explicitly defines a relation between the finite length of the chain and the nonzero energy of the excitations. For positive E we define θ from

$$\frac{\alpha_3}{\alpha_1} = -\frac{\bar{x}}{\bar{y}E} = e^{i\theta}. \tag{39}$$

We recall that α_1 (α_3) is the amplitude of the quasiparticle excitation at the left (right) end of the chain. The corresponding excitations are described by γ_σ, $\tilde{\gamma}_\sigma$ given by Eqs. (19) and (25). In the case of the finite chain we are analyzing here, the exact subgap eigenstate with energy $E > 0$ given by Eq. (38) is a linear combination of the latter ones. It can be described in terms of the annihilation operator of a quasiparticle with this energy as

$$\Gamma_\uparrow = \frac{1}{\sqrt{2}}(\gamma_\uparrow + e^{i\theta}\tilde{\gamma}_\uparrow), \tag{40}$$

where $\gamma_\uparrow$ and $\tilde{\gamma}_\uparrow$ have the same form as in Eqs. (19) and (25), except for the fact that for the finite chain the sum in these equations extends up to L instead of ∞, and then the normalization changes to

$$N = \left[\frac{1 - |z_1|^4}{2\left(1 - |z_1|^{2L}\right)}\right]^{1/2}. \tag{41}$$

As before, a degenerate solution is obtained interchanging spin up and down and changing the sign of both Δ and λ (or by time-reversal operation if $\phi = 0$),

$$\Gamma_\downarrow = \frac{1}{\sqrt{2}}(\gamma_\downarrow + e^{-i\theta}\tilde{\gamma}_\downarrow). \tag{42}$$

Using Eqs. (21) and (26), it can be easily checked that the low-energy eigenstates with negative energy given by Eq. (38) coincide except for an irrelevant factor with the operators $\Gamma^\dagger_\uparrow$ and $\Gamma^\dagger_\downarrow$, transpose conjugate of those defined by Eqs. (40) and (42). This can be expected since taking the transpose conjugate of the equation

$$[\Gamma_\sigma, H] = E\Gamma_\sigma \tag{43}$$

implies $[\Gamma^\dagger_\sigma, H] = -E\Gamma^\dagger_\sigma$.

Here and in what follows, when an operator O satisfies $[O, H] = EO$, with $E \neq 0$, implying $[O^\dagger, H] = -EO^\dagger$ we choose as annihilation operator O for positive E and $O^\dagger$ for negative E, so that the vacuum $|0\rangle_O$ of all these annihilation operators ($O|0\rangle_O = 0$) is the ground state.

IV. LOCALIZATION LENGTH OF THE END STATES

To define the localization length λ_e of the end states, it suffices to consider a chain of infinite length. In this case the energy of the low-energy states is $E = 0$ and it is not necessary to solve the boundary equation to obtain E. The four complex roots of Eq. (11) provide the decay along the chain of the components of the eigenstates of the Hamiltonian, as illustrated in Sec. III. We choose the eigenstates localized at the left end for the following discussion (of course the results are the same choosing the right end). From the four solutions of Eq. (11), only those two with $|z_i| < 1$ contribute to the states localized at the left end. Let us denote as $|z_l|$ the largest of these two absolute values. Clearly this is the one that determines the localization length because at large distances, the probability $p(n)$ of finding a particle at site n is proportional to $|z_l|^{2n}$. Defining as usual the localization length λ_e, from $p(n) \sim \exp(-n/\lambda_e)$ we obtain

$$\lambda_e = \frac{-1}{2\ln|z_l|}. \tag{44}$$

For $\mu = 0$ both roots with $|z_i| < 1$ are given by Eq. (16) and replacing in Eq. (44), λ_e is derived. In general, one has to solve the quartic Eq. (11) and choose the largest $|z_i|$ with the condition $|z_i| < 1$ to obtain the localization length. Following this procedure we derived the results shown in Fig. 2, where the localization length as a function of the chemical potential μ is represented. Note that if z is a solution of Eq. (11), $-z$ is a solution for the opposite value of μ. This and other properties listed above Eq. (11) allows us to restrict the calculations and discussions to all parameters assumed positive, and extend later the result for all signs using the symmetry properties of Eqs. (11) and (44). Starting from $\mu = 0$ and increasing μ, the localization length increases and diverges as the transition to the nontopological phase at $\mu = 2\lambda$ is approached, as expected. In fact, for $\mu = 2\lambda$ there is a double root $z = -i$ of Eq. (11) for $E = 0$. The other two roots are given by

$$z = \frac{i(t^2 + \Delta^2 + \lambda^2 \pm 2\Delta\lambda)}{t^2 + \Delta^2 - \lambda^2 - 2it\lambda}. \tag{45}$$

It is easy to see that for positive Δ and λ, one of these two roots has $|z| > 1$ and the other $|z| < 1$. Then for $\mu \to 2\lambda$, $|z_i| \to 1$, and $\lambda_e \to +\infty$.

To find an analytical expression for the localization length near the topological transition, we expand Eq. (11) up to total second order in $y = z + i$ and $\epsilon = 2\lambda - \mu > 0$ around the point $y = \epsilon = 0$, to obtain after some algebra

$$4(t^2 + \Delta^2)y^2 - 4ty\epsilon + \epsilon^2 = 0. \tag{46}$$

Solving this equation, using Eq. (44) and extending the results to other signs of μ and λ, we get

$$\lambda_e \simeq \frac{t^2 + \Delta^2}{|\Delta|(2|\lambda| - |\mu|)}. \tag{47}$$

While this equation is expected to be valid only near the topological transition, it is a good approximation for the whole range of chemical potential within the topological phase defined by $2|\lambda| > |\mu|$ and $\Delta \neq 0$, as indicated in Figs. 2 and 3. Note that λ_e diverges not only at the boundary $|\mu| \to 2|\lambda|$ of the topological phase, but also for $\Delta \to 0$, which is of course also a boundary of the topological phase and in addition to superconductivity.

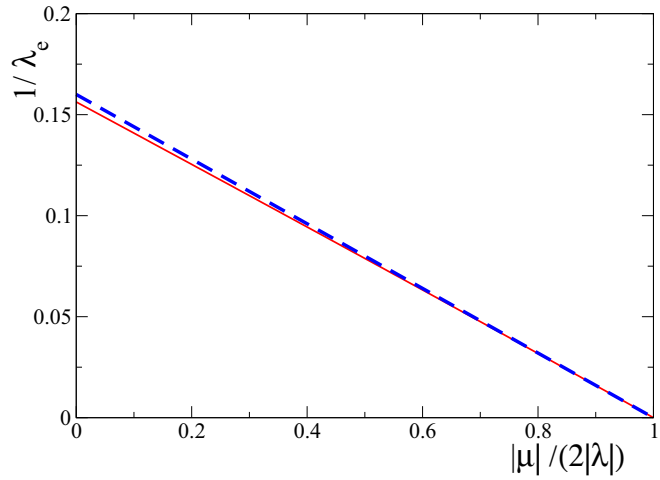

FIG. 2. Full line: Inverse of the localization length as a function of chemical potential. Dashed line corresponds to Eq, (47). Parameters are $t = 1$, $\Delta = 0.5$, $\lambda = 0.2$.

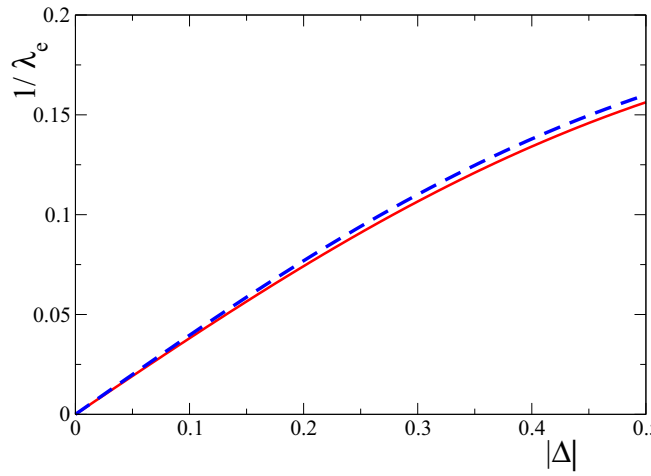

FIG. 3. Full line: Inverse of the localization length as a function of Δ. Dashed line corresponds to Eq, (47). Parameters are $t = 1$, $\mu = 0$, and $\lambda = 0.2$.

For a chain of finite length L, on general physical grounds one expects that the energy E of the low-energy excitations is proportional to $\exp(-L/\lambda_e)$. This is supported by the analytical results of the previous section for $\mu = 0$,

V. SPIN DISTRIBUTION ALONG A FINITE CHAIN

In this section, we calculate the density of spin projection along the Rashba direction z at each site of a finite long chain. We show that for subgap excitation with an odd number of particles, the ground state has a localized spin projection $S_e^z = \pm 1/4$ at each end.

For an even number of particles, the ground state $|g_e\rangle$ can be constructed by applying to the vacuum $|0\rangle_c$ of the $c_{i\sigma}$ operators ($c_{j\sigma}|0\rangle_c = 0$) a product of all annihilation operators of excitations that satisfy

$$[\Gamma_\nu, H] = E_\nu \Gamma_\nu, \tag{48}$$

with positive E_ν. Denoting $\Gamma_{\Theta\nu} = \Theta\Gamma_\nu\Theta^{-1}$, where Θ is the time-reversal operator, the ground state can be written in the form

$$|g_e\rangle = \tilde{N} \prod_\nu \Gamma_\nu \Gamma_{\Theta\nu}|0\rangle_c, \tag{49}$$

where $\tilde{N}$ is a normalization factor.

The z component of the spin operator at site j is

$$S_j^z = \frac{c_{j\uparrow}^\dagger c_{j\uparrow} - c_{j\downarrow}^\dagger c_{j\downarrow}}{2}. \tag{50}$$

Therefore,

$$\begin{aligned}\langle S_i^z\rangle &= \langle g_e|S_i^z|g_e\rangle = \langle g_e|\Theta^{-1}\Theta S_i^z \Theta^{-1}\Theta|g_e\rangle \\ &= -\langle g_e|S_i^z|g_e\rangle = 0,\end{aligned} \tag{51}$$

hence, the expectation value of the spin projection at each site vanishes in the ground state of a chain with an even number of particles.

The ground state for an odd number of particles corresponds to creating the one-particle excitation of lowest energy to $|g_e\rangle$. The energy cost is rather large for all $\Gamma_\nu^\dagger$ except for the subgap states close to $E = 0$ calculated in the previous section (or their generalization for finite μ). The latter have energy $E \sim |z_1|^{L-2}$ decaying exponentially with L. To split the spin degeneracy we assume that a small magnetic field is applied, so that the ground state becomes

$$|g_o\rangle = \Gamma_\uparrow^\dagger |g_e\rangle, \tag{52}$$

where

$$\Gamma_\uparrow = \sum_j (u_j c_{j\uparrow} + v_j c_{j\downarrow}^\dagger), \tag{53}$$

with the coefficients given by Eqs. (19), (25), and (40) for $\mu = 0$. Then,

$$\langle S_i^z\rangle = \langle g_e|\Gamma_\uparrow S_i^z \Gamma_\uparrow^\dagger|g_e\rangle = \langle g_e|[\Gamma_\uparrow, S_i^z]\Gamma_\uparrow^\dagger|g_e\rangle, \tag{54}$$

where we have used Eq. (51) in the last equality.

From Eqs. (50) and (53) we get

$$[\Gamma_\uparrow, S_i^z] = \frac{u_i c_{i\uparrow} + v_i c_{i\downarrow}^\dagger}{2}. \tag{55}$$

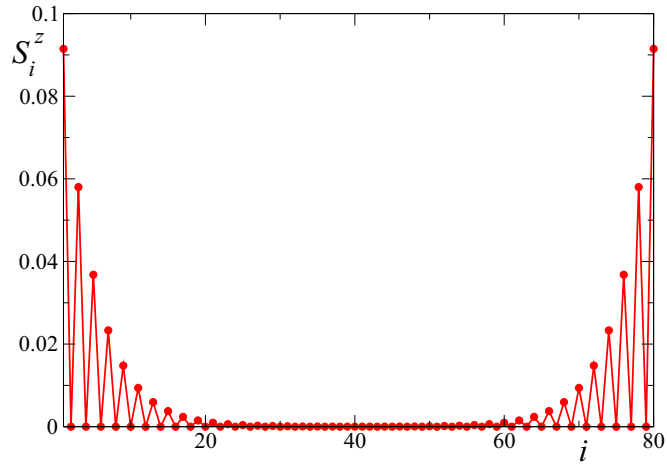

FIG. 4. Spin projection at each site for an odd number of particles and total spin projection 1/2. Parameters are $\mu = 0$, $t = 1$, $\Delta = 0.5$, $\lambda = 0.2$, and $L = 80$.

Using $\langle g_e|\Gamma_\uparrow^\dagger = 0$ we can write Eq. (54) in the form

$$\langle S_i^z\rangle = \langle g_e|\{[\Gamma_\uparrow, S_i^z], \Gamma_\uparrow^\dagger\}|g_e\rangle, \tag{56}$$

and calculating the anticommutators using Eqs. (53) and (55) we finally obtain

$$\langle S_i^z\rangle = \frac{|u_i|^2 + |v_i|^2}{2}. \tag{57}$$

A. Examples

In Fig. 4 we show $\langle S_i^z\rangle$ for an odd number of particles and total spin projection $S_z = \sum_i S_i^z = 1/2$, obtained from the analytical solution, as described in the previous section. We also checked the result by numerical diagonalization of the finite chain. The results are practically identical. The energy of the excitation (which coincides with the difference in energy of the ground state for odd an even particles) is $E = 6.314 \times 10^{-4}$. The numerical energy is higher by $\sim 2 \times 10^{-8}$, which can be ascribed to terms of order E^2 neglected in the analytical treatment.

Clearly half of the total spin projection is localized at each end of the chain and $\langle S_i^z\rangle$ is practically zero in the middle of the chain. Although the physics is different, this is reminiscent of the spin 1/2 excitations at the ends of the $S = 1$ antiferromagnetic chain [39–41]. In addition, there is a marked even-odd oscillation. While $\langle S_i^z\rangle$ decays exponentially as the distance from the ends increase, $\langle S_i^z\rangle$ vanishes exactly at distances equal to an odd number of lattice constants from the ends. This is a particular property of the case $\mu = 0$, but the oscillations remain for finite μ as shown in Figs. 5 and 6.

In Fig. 5 we show $\langle S_i^z\rangle$ as a function of the site, derived form the numerical solution of the chain for the same parameters as before, except for the fact that μ is increased but not too much, so that the system is kept within the topological region $|\mu| < 2|\lambda|$. In this case, according to the calculations of the previous section, the localization length of $\langle S_i^z\rangle$ at the ends of the chain increases from $\lambda_e \simeq 6.4$ to 12.7. This is consistent with the increase in the energy of the excitation by

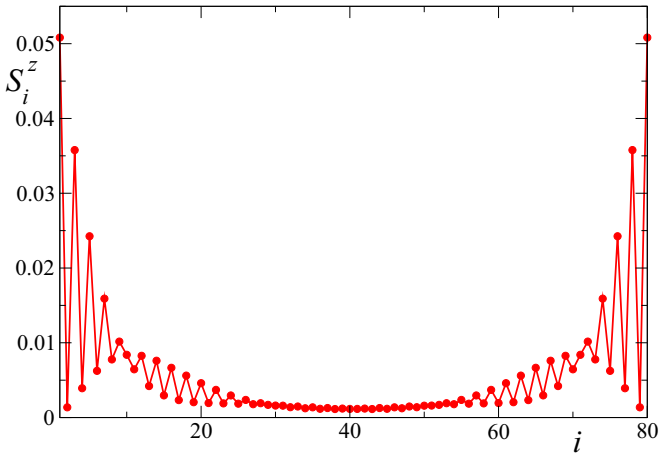

FIG. 5. Same as described in the caption of Fig. 4 except for $\mu = 0.2$.

nearly an order of magnitude to $E = 5.51 \times 10^{-3}$. In contrast to the case $\mu = 0$ for which the energy vanishes for chains of odd length, the energy is similar for one site less ($E = 5.71 \times 10^{-3}$) or one site more ($E = 5.28 \times 10^{-3}$). Actually, for an homogeneous chain, the period of the oscillations is given by the Fermi wavelength of the system without superconductivity, which in turn depends on the chemical potential. For the chosen length of the chain $L = 80$, with order of magnitude comparable to $\lambda_e \simeq 12.7$, the spin excitations at the ends are not well separated. However, the overall trend is similar to the previous case, with larger $\langle S_i^z \rangle$ at the ends and even-odd oscillations. Curiously, while for $i \leqslant 10$, $\langle S_i^z \rangle$ is larger for odd sites, the situation is reversed for $11 \leqslant i \leqslant 30$. A similar situation takes place at the other end replacing i by $L + 1 - i$.

As shown in Fig. 6 if the length of the chain is increased while keeping the same energy parameters, $\langle S_i^z \rangle$ near the ends is practically not affected. However, it is now clear that the spin excitations at both ends are well separated. In this case, the excitation energy is $E = 2.335 \times 10^{-4}$.

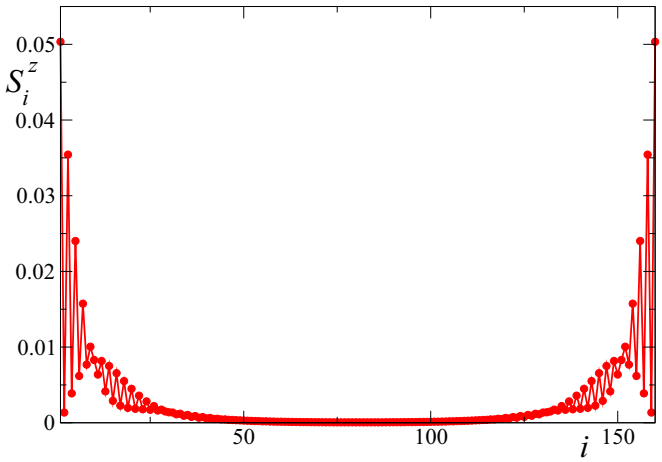

FIG. 6. Same as described in the caption of Fig. 5 except for $L = 160$.

VI. GENERAL PROPERTIES OF THE END STATES

While the specific pattern of the spacial distribution of the spin density or the explicit expression for the localization length depends on the model parameters, as discussed in the previous section, there are other features of the topological phase, which are much more general and only depend on the symmetries of the model. In this section, we focus on such features and we summarize the main properties of the subgap excitations that are valid for any 1D TRITOPS system conserving a given spin porjection, in our case S_z. In particular, Eqs. (27), which we reproduce here for the ease of the reader,

$$\{\gamma_\uparrow, \gamma_\downarrow\} = p, \ \{\tilde{\gamma}_\uparrow, \tilde{\gamma}_\downarrow\} = -p, \tag{58}$$

where p is defined in Eq. (18), have been demonstrated using a continuum formulation in Sec. II of the Supplemental Material of Ref. [23] for $\phi = 0$. We expect them to be generally valid. Extension for $\phi \neq 0$ is trivial using a gauge transformation.

These operators obey the commutation rules with the operator S_z (with z being the direction of the spin-orbit interaction) that were given in Eq. (28).

In the case of a finite chain with length L, the exact subgap eigenstate with energy $E > 0$ given by Eq. (38), is a linear combination of the form given in Eq. (40),

$$\Gamma_\uparrow = \frac{1}{\sqrt{2}}(\gamma_\uparrow + e^{i\theta}\tilde{\gamma}_\uparrow), \tag{59}$$

which satisfies $\{\Gamma_\uparrow, \Gamma_\downarrow\} = 0$. The time-reversal partner is the operator defined in Eq. (42),

$$\Gamma_\downarrow = \frac{1}{\sqrt{2}}(\gamma_\downarrow + e^{-i\theta}\tilde{\gamma}_\downarrow), \tag{60}$$

where θ depends on the model. Generally, going from the infinite chain to the finite one introduces a tunneling between the operators of both ends which can be written as $Ee^{i\theta}$ with E real. This point will be further discussed in the next Section [see Eqs. (63)], whose results are also generic. For the particular model of Sec. II, θ is given by Eq. (39).

The operators Γ_σ annihilate two degenerate excitations (corresponding to $\sigma = \uparrow, \downarrow$) with energy E. Let us also highlight that the structure of the operators Γ_σ defined in Eqs. (40) and (42) imply entanglement of the excitations localized at the left and the right ends of the chain. In fact, we can define two-q-bit states in the basis of Eq. (31) $|l, r\rangle \equiv |lL, rR\rangle$, with $l, r = 0, 1$ and analyze the effect of generating two quasiparticles with $\Gamma_\sigma^\dagger$ on these states. The result is

$$\begin{aligned} \Gamma_\uparrow^\dagger \Gamma_\downarrow^\dagger |0,0\rangle &= \Gamma_\uparrow^\dagger \Gamma_\downarrow^\dagger |1,1\rangle = 0, \\ \Gamma_\uparrow^\dagger \Gamma_\downarrow^\dagger \frac{1}{\sqrt{2}}[|0,1\rangle \pm |1,0\rangle] &= \frac{\overline{p}}{2\sqrt{2}}[(\pm 1 - e^{i\theta})|1,0\rangle \\ &\quad - (1 \mp e^{-i\theta})|0,1\rangle]. \end{aligned} \tag{61}$$

We see that $\Gamma_\uparrow^\dagger \Gamma_\downarrow^\dagger$ does not act on the subspace of product states of single q-bits. However, since the phase θ resulting from Eq. (39) is in general different from $0, \pi$, this operator maps Bell states into combinations of Bell states [38]. Notice that this construction relies on the fact that for finite wires, the energy of the subgap states is finite. In contrast, in the limit of $L \to \infty$, the four two-q-bit states are exactly degenerate

at $E = 0$ and two-quasiparticle excitations can be constructed with any linear combination of these states. These operators obey the commutation rules with the Hamiltonian given by Eq. (43). Finally, it is interesting to notice that these properties are very similar to those discussed in the context of topological phases taking place in 1D spin systems [42,43].

VII. EFFECT OF A MAGNETIC FIELD AT ONE END

A. Quasiparticles

In this section we calculate the spin projection along the Rashba direction at the ends of the chain S_e^z of the ground state and low-energy excitations, as well as the energy of these excitations under the effect of a weak magnetic field (or Ising type interaction) $B > 0$ applied at one end only, parallel to the Rashba direction z. Without loss of generality we assume that the field is applied at the right end of the chain and includes all sites for which $\langle S_i^z \rangle$ is significantly different from 0 for $B = 0$, which means that the length of the region subject to the magnetic field is much larger than the localization length λ_e of the low-energy quasiparticles (see Sec. IV). In particular, it can include the right half of the chain. For concreteness, we assume the latter option and write the Hamiltonian for the superconducting wire in the presence of the external magnetic field B, described by a Zeeman coupling $\Delta_Z = g\mu_B B$ as

$$H_{\rm tot} = H - \Delta_Z S_R^z, \tag{62}$$

where $S_R^z = \sum_{j=L/2}^{L} S_j^z$ is the operator of the total spin projection at the right half of the chain. A sketch is shown in Fig. 1 (see bottom left). Similarly for the left end $S_L^z = S_z - S_R^z$. Alternatively, we can also consider a magnetic island or a magnetic adatom with classical magnetic moment M close to the right end of the chain coupled with the spin through an Ising interaction $H_B = -J S_R^z M$. This is equivalent to the Hamiltonian of Eq. (62) upon identifying $JM \equiv \Delta_Z$. In the case of the magnetic field we assume that its magnitude is much smaller than the critical field of the superconductor. In the case of the magnetic moment, we assume a weak coupling J, such that it interacts with the subgap edge-state excitation but it does not induce low-energy Yu-Shiba-Rusinov states [44] inside the superconducting gap. This assumption implies that we can restrict the effect of the magnetic field to the low-energy in-gap states.

Taking for the moment our analytical solution for $\mu = 0$ using Eqs. (40), (42), (21), and (26) we obtain

$$\begin{aligned} [\gamma_\sigma, H_{\rm tot}] &= E e^{is\theta} \tilde{\gamma}_\sigma, \\ [\tilde{\gamma}_\sigma, H_{\rm tot}] &= E e^{-is\theta} \gamma_\sigma - s\frac{\Delta_Z}{2}\tilde{\gamma}_\sigma, \end{aligned} \tag{63}$$

where $s = 1$ (-1) for spin $\uparrow$ $(\downarrow)$.

For our model with $\mu = 0$, the explicit values of E and $e^{i\theta}$ are given by Eqs. (38) and (39). However, we want to stress that the *form* of Eqs. (63) is generally valid for any TRITOPS chain: the zero modes of the chain in the limit $L \to \infty$, γ_σ at the left and $\tilde{\gamma}_\sigma$ at the right become mixed and split in the finite chain by an effective hopping $Ee^{i\theta}$ (whose detailed value depends on the particular system) for spin up, and time-reversal symmetry implies a hopping $Ee^{-i\theta}$ for spin down. In addition, it can be easily seen from our analytical solution for $\mu = 0$ [see Eq. (30) and the sentence below it], that to linear order in B the end states for $L \to \infty$ do not split if the magnetic field is applied perpendicular to the direction of the Rashba field (z in our notation). For general TRITOPS models a splitting for all directions of the magnetic field is expected, but with a strong anisotropy [45].

Using a Bogoliubov transformation, two annihilation operators can be defined such that

$$[\Gamma_{B,\sigma}, H_{\rm tot}] = E_\sigma \Gamma_{B,\sigma}, \tag{64}$$

with $E_\sigma > 0$. Specifically,

$$\begin{aligned} \Gamma_{B,\sigma} &= \alpha_\sigma \gamma_\sigma + \beta_\sigma e^{is\theta}\tilde{\gamma}_\sigma, \\ E_\sigma &= r - s\frac{\Delta_Z}{4}, \end{aligned} \tag{65}$$

being

$$\begin{aligned} r &= \sqrt{(\Delta_Z/4)^2 + E^2}, \\ \alpha_\uparrow^2 = \beta_\downarrow^2 &= \frac{1}{2} + \frac{\Delta_Z}{4r}, \\ \alpha_\sigma^2 + \beta_\sigma^2 &= 1,\ \alpha_\sigma, \beta_\sigma > 0. \end{aligned} \tag{66}$$

Using Eqs. (27) and (66) one can verify that the operators $\Gamma_{B,\sigma}$ and $\Gamma_{B,\sigma}^\dagger$ obey canonical anticommutation rules.

B. Zeeman splitting

The previous equations make explicit the fact that the finite energy E of the excitations in chains of finite length has associated an hybridization of the localized zero modes. This implies a degree of entanglement between modes localized at opposite ends. Our goal is to analyze the impact of this entanglement in the magnetic response.

The behavior of the quasiparticle excitations given by Eq. (65) have two important limits, which correspond to $\Delta_Z \gg E$ and $\Delta_Z \ll E$.

1. $\Delta_Z \gg E$

This corresponds to strongly localized end states with energy $E \sim 0$. This situation is achieved for very long chains, where the end modes are almost completely decoupled. In this case we can expand r defined in Eq. (66) as $r \sim (\Delta_Z/4)[1 + (4E/\Delta_Z)^2/2]$ and we get

$$\begin{aligned} E_\uparrow &= \frac{2E^2}{\Delta_Z}, \\ E_\downarrow &= \frac{2E^2}{\Delta_Z} + \frac{\Delta_Z}{2}. \end{aligned} \tag{67}$$

In this limit, the operator $\Gamma_{B,\uparrow}$ that corresponds to the one-particle excitation with energy $E_\uparrow$ [see Eq. (65)] tends to the quasiparticle $\gamma_\uparrow$ localized at the left end of the chain [$\alpha_\uparrow^2 \sim 1$, see Eq. (66)], and is not affected by the magnetic field. In turn, the excitation with energy $E_\downarrow$, related to $\Gamma_{B,\downarrow} \sim \tilde{\gamma}_\downarrow$ with energy $E_\downarrow$ corresponds to annihilating a quasiparticle at the right end of the chain with spin down [or creating one with spin up since $\tilde{\gamma}_\uparrow^\dagger = -\bar{p}\tilde{\gamma}_\downarrow$, see Eq. (26)]. This leads to a

decrease of the total energy in $E_\downarrow \sim \Delta_Z/2$, for annihilating an ordinary electron with spin down or creating one with spin up, which is the expected result for an ordinary spin 1/2.

Naturally, the complete spectrum of one-particle excitations also contains those corresponding to the Hermitian conjugate of the above described operators, in particular $\tilde{\gamma}_\downarrow^\dagger \sim \tilde{\gamma}_\uparrow$) with an energy *loss* $E_\downarrow$, so that an ordinary Zeeman splitting is $2E_\downarrow \sim \Delta_Z$ can be inferred from the magnetic-field dependence of the total spectral density of an ordinary electron observed in scanning tunneling spectroscopy, particularly if the STM tip is located near the end of the chain where the magnetic field is applied.

2. $\Delta_Z \ll E$

This case corresponds to a sizable hybridization and entanglement of the end modes. In this other limit we consider $r \sim E[1 + (\Delta_Z/4E)^2/2]$. Hence,

$$E_\uparrow = E\left[1 + \frac{1}{2}\left(\frac{\Delta_Z}{4E}\right)^2\right] - \frac{\Delta_Z}{4},$$
$$E_\downarrow = E\left[1 + \frac{1}{2}\left(\frac{\Delta_Z}{4E}\right)^2\right] + \frac{\Delta_Z}{4}. \quad (68)$$

All low-energy quasiparticles have nearly equal weight at both ends [$\alpha_\uparrow^2 \sim 1/2$, $\beta_\uparrow^2 \sim 1/2$, see Eq. (66)]. As a consequence, the effect of the magnetic field at only one end is reduced by a factor 1/2 with respect to the application of the field in the whole sample. The Zeeman splitting between the one-particle excitations of positive energy (corresponding to annihilation of quasiparticles) is $E_Z = E_\downarrow - E_\uparrow = \Delta_Z/2$, which is half the Zeeman splitting of a spin 1/2.

We believe that this splitting might be observed not only by an STM which senses the one-particle spectral density but also with microwave radiation which induces transtions conserving the number of electrons [34,35]. While the light does not couple directly with the spin, the spin-orbit coupling couples it with the orbital degrees of freedom and circularly polarized light induces transition between stats with angular momentum projection 1/2 and −1/2. As before, the full spectrum of one-particle excitations also contains negative energies with the same moduli as the positive ones described above.

C. Spin polarization

In our model for $\mu = 0$ and large enough chains such that $|z_1|^L \ll 1$, using Eqs. (25) and (41) one obtains that the low-energy part of the spin projection at the right end $S_R^z = \sum_{i=L/2}^{L} S_i^z$ can be written in the form

$$S_R^z \simeq \frac{1}{4}\left(\tilde{\gamma}_\uparrow^\dagger \tilde{\gamma}_\uparrow - \tilde{\gamma}_\downarrow^\dagger \tilde{\gamma}_\downarrow\right), \quad (69)$$

where we have neglected the contribution of the high-energy operators Γ_ξ, $\Gamma_\xi^\dagger$ with $[\Gamma_\xi, H] = E_\xi \Gamma_\xi$, where the subscript ξ labels all operators with $E_\xi \gg E$. It is reasonable to expect that the low-energy part of S_R^z has the same form for a general TRITOPS. Using Eqs. (65) and (26) this part takes the following form, which is the most convenient one for our purpose:

$$S_R^z \simeq \frac{1}{4}\left(\alpha^2 - \beta^2 + 2\beta^2 \Gamma_{B\uparrow}^\dagger \Gamma_{B\uparrow} - 2\alpha^2 \Gamma_{B\downarrow}^\dagger \Gamma_{B\downarrow}\right), \quad (70)$$

where $\alpha = \alpha_\uparrow = \beta_\downarrow > 0$, $\beta = (1-\alpha^2)^{1/2}$ [see Eqs. (66)].

As in Sec. V, the ground state $|g_e\rangle$ for an even number of particles is constructed by applying to the vacuum of the $c_{j\sigma}$ all annihilation operators left invariant by the commutation with the Hamiltonian:

$$|g_e\rangle = \tilde{N} \Gamma_{B\uparrow} \Gamma_{B\downarrow} \prod_\xi \Gamma_\xi |0\rangle_c, \quad (71)$$

where $\tilde{N}$ is a normalization factor.

Using Eqs. (70) and (71) we get

$$\langle g_e | S_R^z | g_e \rangle = \frac{\alpha^2 - \beta^2}{4} = \frac{\Delta_Z}{4\sqrt{(\Delta_Z)^2 + 16E^2}}. \quad (72)$$

For the states with odd number of particles $|g_{o\sigma}\rangle = \Gamma_{B\sigma}^\dagger |g_e\rangle$, one obtains

$$\langle g_{o\sigma} | S_R^z | g_{o\sigma} \rangle = \frac{s}{4}, \quad (73)$$

where $s = 1$ (-1) for spin $\uparrow$ $(\downarrow)$, independently of the applied magnetic field at one end. This fact is expected since for total $S_z = 1/2$ or $-1/2$, there is only one low-energy state and therefore it cannot be modified by a small perturbation. The first correction is of order $(B/E_\xi)^2$ and is neglected in our approach.

In Fig. 7 we present sketches on the two different scenarios expected in the magnetic response of wires with odd and even number of particles, respectively. In Fig. 8 we show the behavior of the spin projection for an even number of particles and the difference between the ground state energies for odd and even number of particles $E(B)$ as a function of the magnetic field. For $B = 0$, $E(0) = E$ and $\langle g_e | S_R^z | g_e \rangle = 0$, consistent with a time-reversal invariant ground state. In general $-1/4 \leqslant \langle g_e | S_R^z | g_e \rangle \leqslant 1/4$ and $0 \leqslant E(B) = E_\uparrow \leqslant E$, and for $\Delta_Z \gg E$, $E(B) \to 0$ and $\langle g_e | S_R^z | g_e \rangle \to 1/4$.

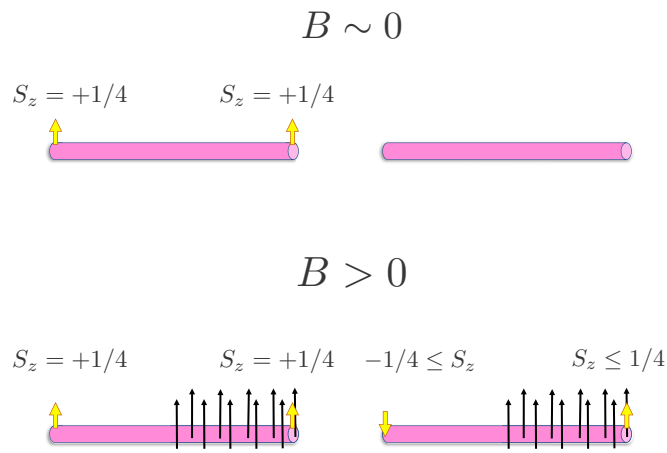

FIG. 7. Sketch of the ground-state expectation value of the spin at the ends when a magnetic field is applied at one of the ends of the wire. The left (right) panels of the figure correspond to a wire with an odd (even) number of particles.

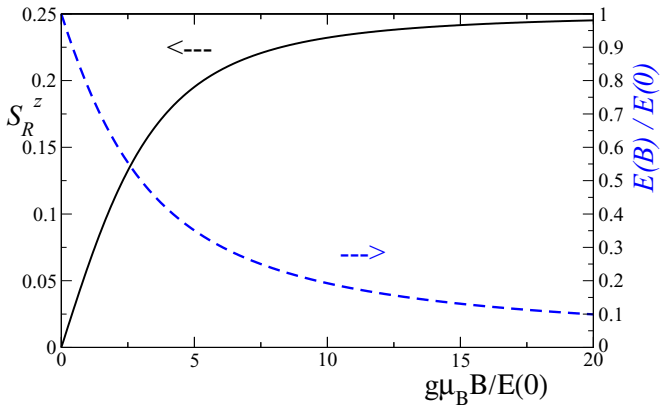

FIG. 8. Ground-state spin projection at the right end of the chain (left scale full line) and first excitation energy (right scale dashed line) as a function of magnetic field applied to the right end.

VIII. SUMMARY AND DISCUSSION

We have calculated the low-energy eigenstates of a finite chain of a time-reversal-invariant topological superconductor numerically and in the particular case of an electron-hole symmetric band ($\mu = 0$) also analytically. The analytical solution allows one to gain insight on the main features of the Majorana zero-energy excitations at the ends of the topological chain and how the end states mix in the finite chain giving rise to low-energy excitations with finite energy.

Using these solutions we have calculated the spin projection for each site i of the chain $\langle S_i^z \rangle$ along the Rashba direction z in finite chains. We show that excitations with total spin projection $S_z = \pm 1/2$ fractionalize in two pieces with $S_e^z = \pm 1/4$ localized at each end of the chain. $\langle S_i^z \rangle$ displays oscillations with an exponential envelope. The decay length of $\langle S_i^z \rangle$ at each end can be calculated solving a quartic equation with complex coefficients for any μ and is well approximated by a simple analytical formula [Eq. (47)].

Although we presented results for a specific model Hamiltonian, all the physical behavior discussed in the present work is generic of TRITOPS wires.

The finite energy excitation E in chains with an odd number of particles with respect to those with even number of particles should be experimentally detectable. In ordinary superconductors, this energy is of the order of the superconducting gap and has been measured in experiments in small islands in which capacitance effects allow researchers to control the number of electrons in small superconducting systems [30]. Furthermore, these experiments permit to tune the chemical potential μ changing the localization length of the states at the end of the chain and the excitation energy E of the quasiparticles entangling both ends. In the present case, E lies deep inside the superconducting gap. Alternatively, scanning tunneling microscope measurements [31–33] could also detect these subgap excitations.

An application of a magnetic field opens other interesting possibilities. The excitation energy E is split by the magnetic field. Applying the field only to one end of the chain would open the possibility of analyzing the response of the fractional spin projections at the ends. We identify two possible scenarios, depending on the amplitude of the Zeeman splitting Δ_Z relative to the energy of the excitations without magnetic field E. In the case of $\Delta_Z \gg E$, which can be easily achieved for very long chains, assuming that the field is applied to right end favoring spin up there, the ground state for an even number of particles has expectation value of the spin projection at the left in the range $-1/4 \leqslant S_L^z \leqslant 0$ and $0 \leqslant S_R^z \leqslant 1/4$ at the right, while the lowest two eigenstates with odd number of particles have $S_L^z = S_R^z = \pm 1/4$. Then, the one-particle excitation energies correspond to flip a fractional spin at the left without energy cost, or flipping it at the right with an energy cost $\Delta_Z/2$, the usual one for creating a spin down.

On the other hand, for $\Delta_Z \ll E$, the entanglement between left and right end excitations manifests itself in the magnetic response. In this case, the ground state for an even number of particles has $S_L^z = S_R^z = 0$, while for odd number of particles still $S_L^z = S_R^z = \pm 1/4$. Clearly, there is a Zeeman splitting of the one-particle excitations equal to $\Delta_Z/2$. This is precisely half the magnitude of the one expected for a ordinary spin 1/2 and reflects the fact that S_z is fractionalized, with $S_e^z = \pm 1/4$ at the ends.

Scanning tunneling microscope measurements akin to those used to investigate Yu-Shiba-Rusinov excitations induced by magnetic impurities should be able to detect these features in the subgap spectrum of TRITOPS wires [31–33]. We believe that also microwave radiation [34,35] can produce transitions between the quasiparticles split by $\Delta_Z/2$ for a small magnetic field.

ACKNOWLEDGMENTS

A.A.A. is sponsored by PIP Grant No. 112-201501-00506 of CONICET and PICT Grant No. 2013-1045 of the ANPCyT. We acknowledge support from CONICET and UBACyT, Argentina, and the Alexander von Humboldt Foundation, Germany.

APPENDIX: SUMMARY OF THE METHOD BY ALASE *et al.* IN THE NAMBÚ FORMALISM

We start by expressing the Hamiltonian of Eq. (1) in terms of Nambu spinors $\psi_j^\dagger = (c_{j\uparrow}^\dagger,\ c_{j\downarrow}^\dagger,\ c_{j\downarrow},\ -c_{j\uparrow})$. The result is

$$H = \sum_{j=1}^{L} \psi_j^\dagger h_0 \psi_j + \sum_{j=1}^{L-1} (\psi_j^\dagger h_1 \psi_{j+1} + \text{H.c.}), \tag{A1}$$

with

$$h_0 = \frac{\mu}{2}\sigma_0 \otimes \tau_z,$$
$$h_1 = -\frac{t}{2}\sigma_0 \otimes \tau_z + i\frac{\lambda}{2}\sigma_z \otimes \tau_z + \Delta\tau_x. \tag{A2}$$

Here, σ_j and τ_j are Pauli matrices acting on the spin and particle-hole degrees of freedom, respectively, while σ_0 and τ_0 are 2×2 unit matrices.

We define the state $|j\rangle$ associated to the Nambu operator ψ_j such that

$$H = \sum_{j=1}^{L} h_0 |j\rangle\langle j| + \sum_{j=1}^{L-1} (h_1 |j\rangle\langle j+1| + \text{H.c.}). \tag{A3}$$

In this notation we define projector operators over bulk (P_B) and boundary ($P_{\rm bou}$) as follows:

$$P_B = \sum_{j=2}^{L-1} |j\rangle\langle j|, \qquad P_{\rm bou} = |1\rangle\langle 1| + |L\rangle\langle L|. \tag{A4}$$

The projector P_B is over all the sites in which all the Hamiltonian matrix elements are contained in the chain, while $P_{\rm bou}$ contains the sites at the left and right ends of the chain. They satisfy $P_B + P_{\rm bou} = 1$.

Following Alase *et al.*, we aim to solve the bulk-boundary eigenvalue problem:

$$P_B H|\Psi\rangle = E P_B|\Psi\rangle, \qquad P_{\rm bou} H|\Psi\rangle = E P_{\rm bou}|\Psi\rangle. \tag{A5}$$

We construct a generalized Bloch state expanding in powers of a complex number z as follows:

$$|\psi^B(z)\rangle = w_z \sum_{j=1}^{L} z^{j-1}|j\rangle. \tag{A6}$$

The latter is represented with a spinor of the form $|\psi^B(z)\rangle = (u_\uparrow(z),\ u_\downarrow(z),\ v_\downarrow(z),\ -v_\uparrow(z))^t$. The coefficients $(u_\sigma(z),\ v_\sigma(z))$ are determined to satisfy

$$P_B[H - E(z)]|\psi^B(z)\rangle = 0. \tag{A7}$$

The rest of the calculation continues in Eqs. (9) to (11). The four eigenstates corresponding to the solution of the bulk problem Eq. (A7) are Nambu states $|\psi_k^B\rangle \equiv |\psi^B(z_k)\rangle$ of the bulk Hamiltonian with $u_{\sigma,k} > 0$ given by Eq. (12) for $\sigma = \uparrow$ and the same equation changing the sign of both Δ and λ for $\sigma = \downarrow$

The last step is to find the solution of the full eigenvalue equation $(H - E)|\Psi\rangle = 0$. To this end we express the state $|\Psi\rangle$ as a linear combination of the bulk eigenstates $|\psi_k^B\rangle$,

$$|\Psi\rangle = \sum \alpha_k |\psi_k^B\rangle. \tag{A8}$$

The coefficients α_k and the energy E are determined to satisfy

$$P_{\rm bou}[H - E]|\Psi\rangle = 0. \tag{A9}$$

The corresponding coefficients are given by Eqs. (13) and (14).

[1] A. Y. Kitaev, Unpaired Majorana fermions in quantum wires, Sov. Phys. Usp. **44**, 131 (2001).

[2] Y. Oreg, G. Refael, and F. von Oppen, Helical Liquids and Majorana Bound States in Quantum Wires, Phys. Rev. Lett. **105**, 177002 (2010)

[3] R. M. Lutchyn, J. Sau, and S. Das Sarma, Majorana Fermions and a Topological Phase Transition in Semiconductor-Superconductor Heterostructures, Phys. Rev. Lett. **105**, 077001 (2010).

[4] V. Mourik, K. Zuo, S. M. Frolov, S. R. Plissard, E. P. A. M. Bakkers, and L. P. Kouwenhoven, Signatures of Majorana fermions in in hybrid superconductor-semiconductor nanowire devices, Science **336**, 1003 (2012).

[5] A. Das, Y. Ronen, Y. Most, Y. Oreg, M. Heiblum, and H. Shtrikman, Zero-bias peaks and splitting in an Al-InAs nanowire topological superconductor as a signature of Majorana fermions, Nat. Phys. **8**, 887 (2012).

[6] S. M. Albrecht, A. P. Higginbotham, M. Madsen, F. Kuemmeth, T. S. Jespersen, J. Nyg, P. Krogstrup, and C. M. Marcus, Exponential protection of zero modes in Majorana islands, Nature **531**, 206 (2016).

[7] M. Deng, S. Vaitiekenas, E. Hansen, J. Danon, M. Leijnse, K. Flensberg, J. Nygard, P. Krogstrup, and C. Marcus, Majorana bound state in a coupled quantum-dot hybrid-nanowire system, Science **354**, 1557 (2016).

[8] H. J. Suominen, M. Kjaergaard, A. R. Hamilton, J. Shabani, C. J. Palmstrøm, C. M. Marcus, and F. Nichele, Zero-Energy Modes from Coalescing Andreev States in a Two-Dimensional Semiconductor-Superconductor Hybrid Platform Phys. Rev. Lett. **119**, 176805 (2017).

[9] L. Fu and C. L. Kane, Josephson current and noise at a superconductor/quantum-spin-Hall-insulator/superconductor junction, Phys. Rev. B **79**, 161408(R) (2009).

[10] S. Nadj-Perge, I. K. Drozdov, J. Li, H. Chen, S. Jeon, J. Seo, A. H. MacDonald, B. A. Bernevig, and A. Yazdani, Topological matter: Observation of Majorana fermions in ferromagnetic atomic chains on a superconductor, Science **346**, 602 (2014).

[11] E. Dumitrescu and S. Tewari, Topological properties of time reversal symmetric Kitaev chain and applications to organic superconductors, Phys. Rev. B **88**, 220505(R) (2013)

[12] F. Zhang, C. L. Kane, and E. J. Mele, Time-Reversal-Invariant Topological Superconductivity and Majorana-Kramers Pairs, Phys. Rev. Lett. **111**, 056402 (2013).

[13] A. Keselman, L. Fu, A. Stern, and E. Berg, Inducing Time-Reversal-Invariant Topological Superconductivity and Fermion Parity Pumping in Quantum Wires, Phys. Rev. Lett. **111**, 116402 (2013).

[14] A. Haim, A. Keselman, E. Berg, and Y. Oreg, Time-reversal-invariant topological superconductivity induced by repulsive interactions in quantum wires, Phys. Rev. B **89**, 220504(R) (2014)

[15] A. Haim, K. Wölms, E. Berg, Y. Oreg, and K. Flensberg, Interaction-driven topological superconductivity in one dimension, Phys. Rev. B **94**, 115124 (2016)

[16] Ch. Reeg, C. Schrade, J. Klinovaja, and D. Loss, DIII Topological superconductivity with emergent time-reversal symmetry, Phys. Rev. B **96**, 161407 (2017)

[17] S. Nakosai, J. K. Budich, Y. Tanaka, B. Trauzettel, and N. Nagaosa, Majorana Bound States and Nonlocal Spin Correlations in a Quantum Wire on an Unconventional Superconductor, Phys. Rev. Lett. **110**, 117002 (2013).

[18] S. Deng, L. Viola, and G. Ortiz, Majorana Modes in Time-Reversal Invariant S-Wave Topological Superconductors, Phys. Rev. Lett. **108**, 036803 (2012).

[19] S. B. Chung, J. Horowitz, and X-L. Qi, Time-reversal anomaly and Josephson effect in time-reversal-invariant topological superconductors, Phys. Rev. B **88**, 214514 (2013).

[20] J. Klinovaja, A. Yacoby, and D. Loss, Kramers pairs of Majorana fermions and parafermions in fractional topological insulators, Phys. Rev. B **90**, 155447 (2014).

[21] C. Schrade, A. A. Zyuzin, J. Klinovaja, and D. Loss, Proximity-Induced π Josephson Junctions in Topological Insulators and Kramers Pairs of Majorana Fermions, Phys. Rev. Lett. **115**, 237001 (2015)

[22] J. Li, W. Pan, B. Andrei Bernevig, and Roman M. Lutchyn, Detection of Majorana Kramers Pairs Using a Quantum Point Contact, Phys. Rev. Lett. **117**, 046804 (2016)

[23] A. Camjayi, L. Arrachea, A. Aligia, and F. von Oppen, Fractional Spin and Josephson Effect in Time-Reversal-Invariant Topological Superconductors, Phys. Rev. Lett. **119**, 046801 (2017).

[24] C. Schrade and L. Fu, Parity-controlled 2π Josephson Effect Mediated by Majorana Kramers Pairs, Phys. Rev. Lett. **120**, 267002 (2018)

[25] A. Chew, D. F. Mross, and Jason Alicea, Fermionized parafermions and symmetry-enriched Majorana modes, Phys. Rev. B **98**, 085143 (2018).

[26] M. Mashkoori, A. G. Moghaddam, M. H. Hajibabaee, A. M. Black-Schaffer, and F. Parhizgar, Impact of topology on the impurity effects in extended s-wave superconductors with spin-orbit coupling, arXiv:1805.11885.

[27] A. Haim and Y. Oreg, Time-reversal-invariant topological superconductivity, arXiv:1809.06863

[28] A. Alase, E. Cobanera, G. Ortiz, and L. Viola, Exact Solution of Quadratic Fermionic Hamiltonians for Arbitrary Boundary Conditions, Phys. Rev. Lett. **117**, 076804 (2016)

[29] A. Alase, E. Cobanera, G. Ortiz, and L. Viola, Generalization of Bloch's theorem for arbitrary boundary conditions: Theory, Phys. Rev. B **96**, 195133 (2017).

[30] P. Lafarge, P. Soyez, D. Esteve, C. Urbina, and M. H. Devoret, Measurement of the Even-Odd Free-Energy Difference of an Isolated Superconductor, Phys. Rev. Lett. **70**, 994 (1993).

[31] A. Yazdani, B. A. Jones, C. P. Lutz, M. F. Crommie, and D. M. Eigler, Probing the local effects of magnetic impurities on superconductivity, Science **275**, 1767 (1997).

[32] B. W. Heinrich, J. I. Pascual, and K. J. Franke, Single magnetic adsorbates on s-wave superconductors, Prog. Surf. Sci. **93**, 1 (2018).

[33] N. Hatter, B. W. Heinrich, D. Rolf, and K. J. Franke, Scaling of Yu-Shiba-Rusinov energies in the weak-coupling Kondo regime, Nat. Commun. **8**, 2016 (2017)

[34] C. Janvier, L. Tosi, L. Bretheau, Ç. Ö. Girit, M. Stern, P. Bertet, P. Joyez, D. Vion, D. Esteve, M. F. Goffman, H. Pothier, and C. Urbina, Coherent manipulation of Andreev states in superconducting atomic contacts, Science **349**, 1199 (2015).

[35] M. Hays, G. de Lange, K. Serniak, D. J. van Woerkom, D. Bouman, P. Krogstrup, J. Nygard, A. Geresdi, and M. H. Devoret, Direct Microwave Measurement of Andreev-Bound-State Dynamics in a Semiconductor-Nanowire Josephson Junction, Phys. Rev. Lett. **121**, 047001 (2018)

[36] A. Zazunov, A. Iks, M. Alvarado, A. L. Yeyati, and R. Egger, Josephson effect in junctions of conventional and topological superconductors, arXiv:1801.10343

[37] The terms proportional to α_3 in Eqs. (33) and (34) are proportional to $\bar{z}_1^{L-2} + (-\bar{z}_1)^{L-2}$. For odd L they vanish and the excitations for both ends continue to be decoupled with $E = 0$.

[38] C. W. J. Beenaker, Electron-hole entanglement in the Fermi sea, *Proceedings of the International School of Physics, Enrico Fermi*, Vol. 162: Quantum computers, algorithms, and chaos, (IOS Press, Amsterdam, 2006), p. 307.

[39] S. Miyashita and S. Yamamoto, Effects of edges in S=1 Heisenberg antiferromagnetic chains, Phys. Rev. B **48**, 913 (1993).

[40] S. White and D. A. Huse, Numerical renormalization-group study of low-lying eigenstates of the antiferromagnetic S=1 Heisenberg chain, Phys. Rev. B **48**, 3844 (1993).

[41] C. D. Batista, K. Hallberg, and A. A. Aligia, Specific heat of defects in the Haldane system Y_2BaNiO_5, Phys. Rev. B **58**, 9248 (1998).

[42] X. Chen, Z-C. Gu, Z-X. Liu, and X-G. Wen, Symmetry protected topological orders and the group cohomology of their symmetry group, Phys. Rev. B **87**, 155114 (2013)

[43] B. Zeng, X. Chen, D-L. Zhou, and X-G. Wen, Quantum information meets quantum matter, arXiv:1508.02595

[44] L. Yu, Bound state in superconducors with paramagnetic impurities, Acta Physica Sinica **21**, 75 (1965); H. Shiba, Classical spins in superconductors, Progr. Theoret. Phys. **40**, 435 (1968); A. I. Rusinov, On the theory of gapless superconductivity in alloys containing paramagnetic impurities, Sov. Phys. JETP **29**, 1101 (1969).

[45] E. Dumitrescu, J. D. Sau, and S. Tewari, Magnetic field response and chiral symmetry of time-reversal-invariant topological superconductors, Phys. Rev. B **90**, 245438 (2014).